Current Status of LS-DYNA® Iso-geometric Analysis in Crash Simulation

Yijung Chen[1], Shih-Po Lin[1], Omar Faruque[1], Jim Alanoly[1], Mohammed El-Essawi[1] and Ragu Baskaran[1]

1. Ford Motor Company

Abstract

*This paper reports a current implementation of Iso-geometric Analysis (IGA) in crash simulation. Several crash critical enhancements of IGA had been proposed by Ford and implemented by LSTC. Such examples include the fix of shear-locking of Mindlin-Reissner shell and the implementation of attached node to NURBS patch. The benchmark of IGA Mindlin-Reissner shell reveals the existence of mild shear-locking in the default full integration scheme. This problem had been fixed in the new option of selected reduced integration. The non-interpolatory nature of NURBS control points makes them not suitable for CAE nodal operations. The attached-node feature to NURBS patch was then created to output nodal time history and to apply nodal force or nodal constraint for IGA model. To exhibit the superiority of IGA performance, an example of curved component was developed to demonstrate the benefit of exact geometry in computational analysis. A crash-can sled model with fixed rigid wall was built to test IGA features which used in frontal crash. This sled model contains all required ingredients – IGA contacts rigid wall, IGA self-contact, meshless spot-welds connecting to NURBS patch, rigid body-IGA connection, gravity loading, nodal acceleration and the compatibility of *MAT_024 plasticity model with IGA model – to evaluate the performance of IGA in crash safety analysis. The implementation of Bezier extraction to interface with other advanced spline functions and the development of IGA-FE hybrid model for future crash safety development are also addressed.*

KEY WORDS: LS-DYNA; IGA; NURBS; Crash Simulation; Mindlin-Reissner plate; Kirchhoff-Love plate; Shear Locking;

1. Introduction

In the past decade, Iso-geometric Analysis (IGA) [1-5] has been developed in Computer-Aided Engineering (CAE) for numerical simulations. The concept of IGA is to introduce the basis functions used in Computer-Aided Design (CAD) geometry to solve the partial differential equations (PDE's), or in terms of industrial application, to solve mechanical problems via numerical simulations. Improved accuracy and the promise of seamless integration of CAD and CAE are the major driving forces behind the development of IGA technology. The CAD geometry and the CAE model can easily communicate with each other through a basis functions called NURBS (Non-Uniform Rational B-Spline). The basis functions of the CAD geometry are adopted as the so-called shape functions in the finite element analysis (FEA) for the construction of the model geometry and the physical fields (such as displacement or temperature). To distinguish from the conventional finite element analysis (FEA) for the adoption of the CAD functions, the term Iso-geometric Analysis (IGA) is used in this paper for numerical simulations by using the CAD basis functions.

In IGA, the NURBS functions, which are ubiquitous in CAD industry, were firstly introduced into CAE modeling by Hughes et al. [1]. With the adoption of NURBS functions, exact geometry can be preserved in the CAE model, since the same basis is used in the CAD geometry. Furthermore, the NURBS functions have some advantages over the Lagrange type polynomials used in FEA, such as higher smoothness and discretization with adequate uniformity. Three

different types of refinement schemes for NURBS patches can be implemented, including the h- and p- refinements, which are commonly used in FEA, and the so-called k-refinement [1] where the continuity of the NURBS basis functions can be elevated with the increase of the approximation order.

There are two ways of implementing an Iso-geometric analysis algorithm into a finite element code. In the first approach, the NURBS functions are used directly. Since NURBS functions, unlike the shape functions in traditional finite element, are spanning more than one quadrature element, an entirely new solver algorithm is required to handle them. In the second approach, the concept of Bézier extractions [15-16] from NURBS or other advanced spline functions are used to define the new basis functions spanning only a single quadrature element. As such, traditional finite element solvers can be used requiring changes of the shape function in element user subroutines only. For industrial applications of IGA, LSTC has implemented both of these IGA approaches into their solver LS-DYNA. The development of corresponding pre-processing and post-processing functionalities in LS-PrePost® to support these new IGA features are mostly completed and the rests are under negotiation of prioritization for future direction.

For the first approach, two-dimensional NURBS & trimmed NURBS elements are implemented into LS-DYNA for Mindlin-Reissner [6] and Kirchhoff-Love [7] plate theories. A trimmed NURBS geometry can be generated using LS-PrePost to avoid the time-consuming mesh generation and provide some numerical benefits, such as keeping the smoothness of NURBS functions, in the IGA simulation. For auto industry, the integration of CAD and CAE, the identity of CAD and CAE geometries and the superiority of NURBS functions over finite element shape functions will help reduce the cost of the design cycles and provide better efficiency and accuracy in CAE simulations.

In this paper, we will focus on the crash safety simulations with NURBS-based IGA using the first approach only. The current status of the LS-DYNA and LS-PrePost will be reported. Some issues and characteristics in NURBS-based IGA will be discussed: 1. Shear locking effect due to the two-field (displacement and rotation) approximation in Mindlin-Reissner plate. 2. Geometric exactness of IGA. 3. Multiple-patch NURBS model. 4. Some other functionalities of IGA required to support crash modeling. Numerical experiments of crash safety simulations were conducted. A front crash-can of simple geometry was modelled by using non-uniform rational B-spline (NURBS) patches. The simulations were performed with trimmed and untrimmed NURBS-based IGA and the numerical results of IGA were verified through the comparison with the results from finite element analysis in LS-DYNA. Some remaining issues such as the section force calculation and the computational efficiency in LS-DYNA IGA will be also discussed. At the end of this paper, conclusions will be made for the current status of LS-DYNA IGA.

2. The Formulation of Non-Uniform Rational B-Spline functions

2.1. B-Spline basis functions

A B-spline curve can be expressed by the linear combination of the products of the B-spline basis functions, $N_{i,p}(\xi)$ and the control points, $\mathbf{P}_i$:

$$\mathbf{C}(\xi) = \sum_{i=1}^{n} N_{i,p}(\xi)\mathbf{P}_i \tag{1}$$

where the subscript *i* denotes the ordering number of the B-spline basis function and *p* refers to its approximation order. A *B*-spline basis function is defined by the knot vector in the parametric space written as $\Xi = \{\xi_1 \quad \xi_2 \quad \cdots \quad \xi_{n+p+1}\}$ where ξ_i is the value of the *i*-th knot, *i = 1,2,3,…, n+p+*1 and *n* is the total number of *B*-spline basis functions. If knots in a knot vector are equally spaced, they are called *uniform*; otherwise, they are called *non-uniform*. The *i*-th *B*-spline basis function in one dimension can be defined using the Cox-de Boor recursion formula **Error! Reference source not found.**], starting with piecewise constants (*p*=0):

$$N_{i,0}(\xi) = \begin{cases} 1 & , \xi_i \le \xi \le \xi_{i+1} \\ 0 & , \text{otherwise} \end{cases}$$
$$N_{i,p}(\xi) = \frac{\xi - \xi_i}{\xi_{i+p} - \xi_i} N_{i,p-1}(\xi) + \frac{\xi_{i+p+1} - \xi}{\xi_{i+p+1} - \xi_{i+1}} N_{i+1,p-1}(\xi), \quad p \ge 1 \tag{2}$$

The support of $N_{i,p}(\xi)$ is compact with the interval $[\xi_i, \xi_{i+p+1})$, which is termed as the *knot span*. If a knot has multiplicity *k*, the basis functions at this knot are C^{p-k}-continuous. Similarly, the order of continuous derivative decreases *k* times for knots or control points with multiplicity of *k*. For multi-dimensional approximations, the *B*-spline basis functions, $\mathbf{B}_\alpha(\boldsymbol{\xi})$, can be constructed by using the tensor product of one dimensional case.

$$\mathbf{B}_\alpha(\boldsymbol{\xi}) = \prod_{d=1}^{m} {}^{d}N_{\alpha_d, p_d}\left({}^{d}\xi\right) \tag{3}$$

Here, $\alpha = (\alpha_1, \alpha_2, \ldots, \alpha_m)$ denotes the *m*-dimensional index; $\boldsymbol{\xi} = \left\{{}^{1}\xi, {}^{2}\xi, \ldots, {}^{m}\xi\right\}$; p_d, ${}^{d}\xi$, and ${}^{d}N_{\alpha_d, p_d}$ are the order of the *B*-spline function, parametric coordinates, and the B-spline basis, respectively, in the parametric direction *d*. The multivariate B-spline geometry can be expressed as:

$$\mathbf{S}(\boldsymbol{\xi}) = \sum_{\alpha} \mathbf{B}_\alpha(\boldsymbol{\xi}) \mathbf{P}_\alpha \tag{4}$$

2.2. Non-Uniform Rational B-Spline basis functions

Although B-spline basis has some superiority over FE basis, there are still some deficiencies in B-spline approximation. Some commonly used CAD geometries, such as conic shapes (circles, ellipses, sphere, and etc.), cannot be exactly represented by using B-spline basis functions. Hence, the so-called Non-uniform Rational B-spline (NURBS) basis functions were introduced

to CAD and CAE. The NURBS geometry can be represented by using the following mathematical formulation:

$$\mathbf{Q}(\xi) = \sum_{\alpha} \mathbf{R}_{\alpha}(\xi)\mathbf{P}_{\alpha} \tag{5}$$

where $\mathbf{R}_{\alpha}(\xi) = \prod_{d=1}^{m} {}^{d}R_{\alpha_d, p_d}\left({}^{d}\xi\right)$, ${}^{d}R_{\alpha_d, p_d}$ is the rational B-spline basis in the parametric direction *d* and the one-dimensional rational B-spline basis functions can be expressed as

$$R_{i,p}(\xi) = \frac{N_{i,p}(\xi)w_i}{\sum_{k=1}^{n} N_{k,p}(\xi)w_k} \tag{6}$$

in which w_i is the weight of the *i*-th control point, which can be treated as the value of the control point in the *(d*+1*)*-th dimension. NURBS based functions possess the property of partition of unity which has been proved to be the minimum requirement for algebraic convergence. However, the NURBS basis functions do not possess the Kronecker delta properties, meaning the control points are not the physical points. Consequently, additional efforts are required by using the NURBS formulation in (5). Moreover, an *affine transformation* is applied to a *B*-spline or NURBS entity by applying it to the control points.

3. Some basics of Bezier extraction approach

Spline functions such as NURBS and T-splines are defined over the entire domain of a patch and thereby span more than one element. This is contrary to finite element method where adopted Lagrangian shape functions spans over an element only. As a result, NURBS or other Spline based IGA algorithms cannot be implemented directly using the existing framework of an FEA code. This issue is resolved using Bernstein polynomial basis functions which span a single element, instead of B-Spline basis functions to represent the NURBS or other Spline curves.

Bernstein polynomials basis functions can be written as

$$B_{i,p}(\xi) = \frac{1}{2^p}\binom{p}{i-1}(1-\xi)^{p-i+1}(1+\xi)^{i-1} \tag{7}$$

The above equation expresses the *i*-th term of the *p*-th order Bernstein polynomial $B_{i,p}(\xi)$ in one dimension, where

$$\binom{p}{i-1} = \frac{p!}{(i-1)!(p-i+1)}, \quad 1 \le i \le p+1 \tag{8}$$

Figure 1 shows the shapes of different orders of the 1-D Bernstein polynomials.

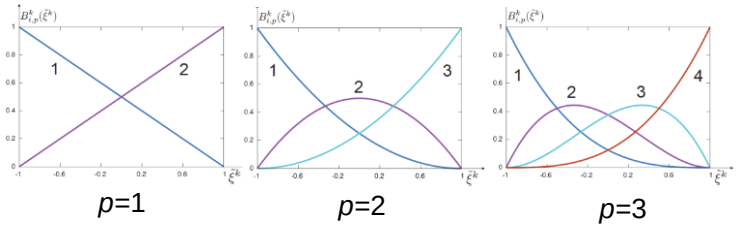

Figure 1. Different orders of Bernstein polynomials

The Bézier extraction operator maps the Bernstein polynomial basis functions to the B-spline basis functions and can be expressed as follows:

$$N_a^e(\xi) = \sum_{b=1}^{(p+1)^{d_p}} C_{a,b}^e B_b(\xi) \tag{9}$$

where $N_a^e(\xi)$ is the chosen spline basis function within an element e, $c_{a,b}^e$ is the Bezier extraction operator and d_p is the dimensionality of the chosen spline. Equation (9) shows that the chosen spline basis functions can be exactly represented by the Bernstein polynomials.

4. Current Status of LS-PrePost and LS-DYNA

4.1. Shear Locking Effect of Mindlin-Reissner Plate in NURBS-based IGA

It is well known that under the assumption of Mindlin-Reissner plate theory, two-field approximation (displacement and rotation) induced the so-called shear locking effect. In FEA, a lot of studies have been done for resolving the shear locking effects. In the literature, some approaches such as selective reduced integration **Error! Reference source not found.**] or assumed strain **Error! Reference source not found.**] approaches have been widely implemented to resolve the shear locking effect. In NURBS-based IGA, similar approaches were considered to relive the shear locking effect **Error! Reference source not found.Error! Reference source not found.**]. In the LS-DYNA IGA, a selective reduced integration method was introduced to the discretized mathematical model. Here a simply supported Timoshenko beam is considered to demonstrate the shear locking effect in IGA as shown in Figure 2, where the material properties

and loading conditions are also shown in the figure. A 2-D IGA model of Mindlin-Reissner plate was constructed for the simulation of the problem.

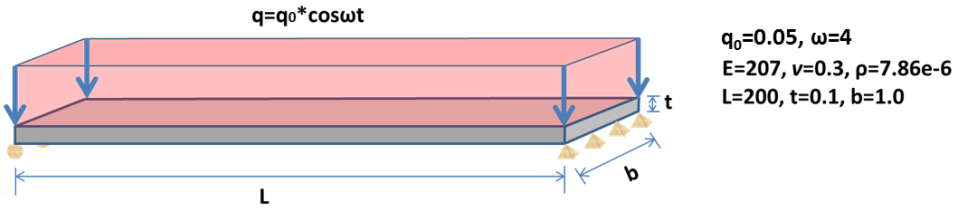

Figure 2. Simply supported Timoshenko beam

The analytical solution of the mid-span deflection can be expressed as a Fourier-type series:

$$d_{mid} = \sum_{m=1}^{\infty} A_m \sin\left(0.5\lambda_m L\right)\left(\cos\Omega t - \cos\omega_m t\right) \tag{10}$$

where

$$\begin{aligned}
&A_m = \left[\left(2m-1\right)\pi\left(C_1\lambda_m^4 - C_2\Omega^2\lambda_m^2 + C_3\Omega^4 - C_4\Omega^2\right)\right]^{-1} \\
&\lambda_m = \frac{2m-1}{L}\pi,\ \omega_m = \sqrt{\frac{b_m - \sqrt{b_m^2 - 4ac_m}}{2a}},\ a = \left[\frac{\rho\left(1+r\right)}{E}\right]^2 - \left[\frac{\rho\left(1-r\right)}{E}\right]^2 \\
&b_m = \frac{4\rho bt}{EI} + 4\lambda_m^2\frac{\rho\left(1+r\right)}{E},\ c_m = 4\lambda_m^4,\ r = \frac{6E}{5G},\ k = 1 - \frac{6\Omega^2\rho I}{5Gbt} \\
&C_1 = \frac{EI}{k},\ C_2 = \frac{\rho I\left(1+r\right)}{k},\ C_3 = \frac{6\rho^2 GI}{5k},\ C_4 = \frac{\rho bt}{k}
\end{aligned} \tag{11}$$

In which E and G are the Young's and shear moduli, ρ is the density, b and t are the beam width and depth, and I is the second moment of inertia. Figure 3 shows the comparison of the results from FEA (form 16), IGA with full integration and IGA with selective reduced integration. As can be seen in Figure 3, when selective reduced integration method was utilized the shear locking effect is relieved. However, the solution of FEA is still more accurate than IGA even some additional effort has been done. This is because FEA is linear polynomial based and its shear locking can be completely removed through the technique of selective reduce integration while high order polynomial based methods, including IGA, the high order locking modes cannot be completely removed by using reduced integration or assumed strain approaches.

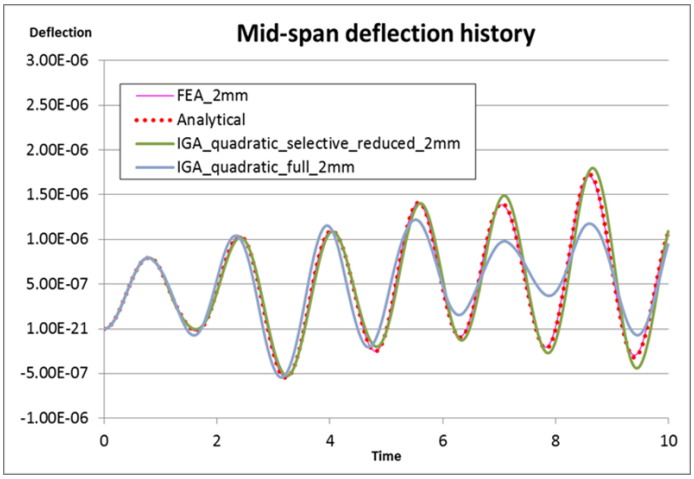

Figure 3. Comparison among FEA and IGA

4.2. CAD-CAE communication in LS-PrePost

To integrate CAD and CAE, a very important step is to convert the CAD geometry to the CAE model. In LS-PrePost, the CAD geometry can be easily converted to trimmed NURBS patches. Here we have the 3-D CAD geometry of a front horn as shown in Figure 4. The procedure of the conversion from CAD geometry to NURBS patches is illustrated in Figure 5. As can be seen, to construct the 2D-CAD model, we firstly generate the mid-surface. For this step, some preprocessing software such as HyperMesh can be used to generate the mid-surfaces. However, a single piece of the front horn is consisted of multiple surfaces. This might cause some problems, such as reducing the continuity on NURBS patch boundaries, in the IGA model. To avoid this, the multiple surfaces can be combined into a single patch by using LS-PrePost and consequently, single NURBS patches can be constructed. In the IGA model, the holes and the complicated outer boundaries of the front horn can be defined by using trimming lines. Eventually, the CAE model can be constructed and the simulation can be conducted. Note that, in the simulation, trimmed NURBS functions are used to represent the displacement and rotation fields.

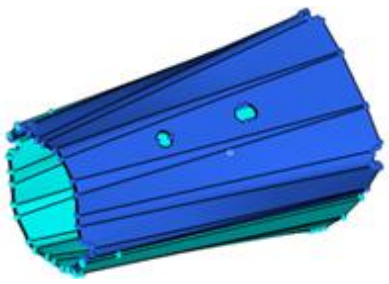

Figure 4. 3-D CAD geometry of a front horn

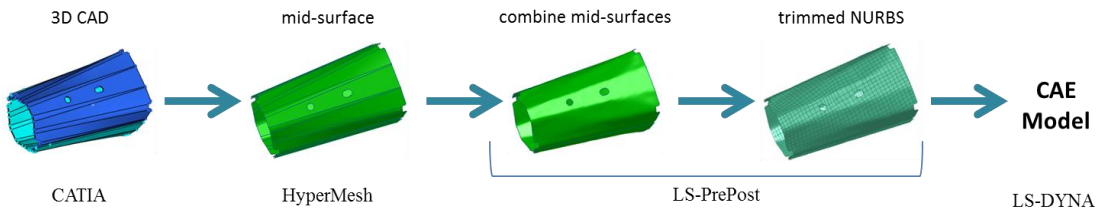

Figure 5. The procedure of converting CAD geometry to the IGA model

Figure 6 shows the details of the trimmed NURBS discretization converted from the CAD geometry, where the control points out of the trimming lines will be eliminated during the simulations. The CAD-CAE conversion functionality of LS-PrePost hugely facilitates the process of CAE simulation. The generated NURBS mesh in the physical domain is quasi-uniform, which offers some advantages in numerical simulations. For example, the critical time step size won't be too small in the explicit dynamic analysis, since the minimum mesh size can be maintained at some appropriate size. Severe mesh distortion can be either avoided or relieved due to the high smoothness of the NURBS basis functions and regularity of the NURBS discretization. More importantly, the CAD-CAE communication in IGA will highly reduce the time of design cycles, since only little effort is required to convert the CAD model to the CAE model when the design is changed.

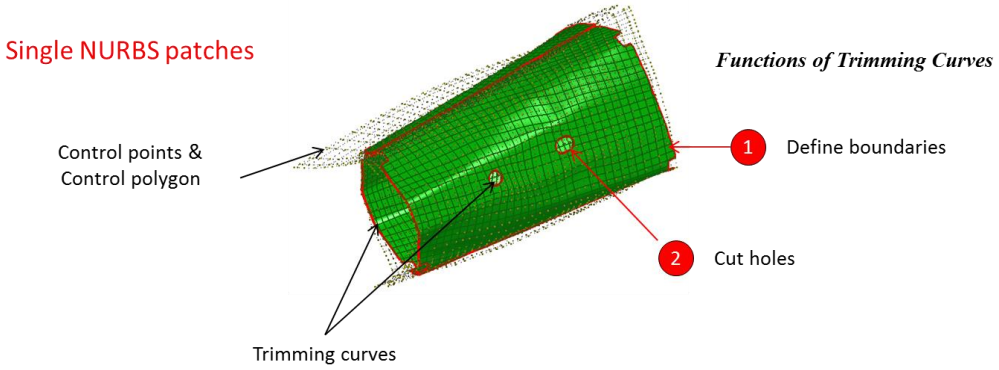

Figure 6. The trimmed NURBS model of the front horn

4.3. Geometric exactness

Since IGA is based on the CAD functions, the geometry description of IGA is consistent with CAD. Therefore, we can claim that the geometry of the CAE model is exact due to the fact that the CAD geometry is considered "exact" in the design stage. Furthermore, the NURBS functions can exactly represent any conic shape which is commonly used for applications. In terms of CAE

simulations, IGA can offer benefits not only the geometric exactness but also the accuracy in the numerical simulations due to the exact representation of the model. Here, we consider a cantilever beam subjected to prescribed displacement on the right end as shown in Figure 7. The cross- section profile with its dimensions and the material properties are also shown in the figure.

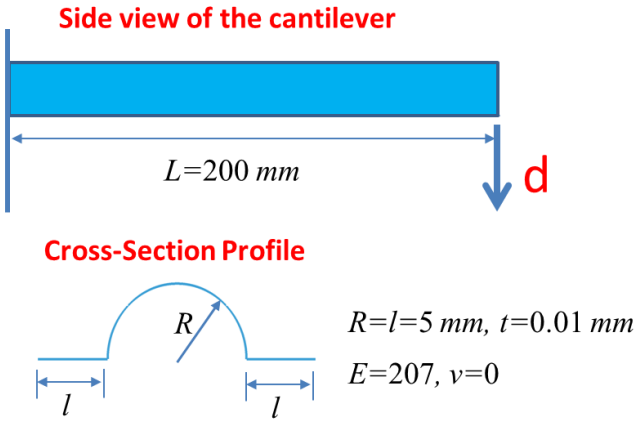

Figure 7. A cantilever subjected to a prescribed tip displacement

The cross section consists of two flat flanges and a half-circle which can be exactly represented by the NURBS basis functions but not FEA shape functions. To show the superiority of IGA, we compare the geometries of the models of FEA and IGA under different discretization as shown in Figure 8. As can be seen, IGA model always represents the exact geometry while FEA only provides approximated ones. To provide sufficient accuracy of the approximation of geometry, it's required at least (17+16)x101 nodes in the FEA model. Note that the number "17" with the underline is the number of nodes used for the half circle of the cross section.

To further compare the performance in terms of CAE modeling, the numerical results of the tip deflection under different discretization of linear FEA and quadratic IGA are shown in Figure 9. For avoiding complexity, the cantilever is considered as a plate structure under the Kirchhoff-Love assumption, meaning the shear deformation is neglected since small thickness is adopted in this case. The analytical solution of this example can be expressed as follows:

$$
\begin{aligned}
&F = K_s d, \quad K_s = \frac{3EId}{L^3} \\
&I = \frac{2}{3} l t^3 + \frac{1}{2} \pi R^3 t - C^2 A \\
&\mathrm{A} = 2lt + \pi R t, \quad C = \frac{2R^2 t + l t^2}{A}
\end{aligned}
\tag{12}
$$

where K_s is the equivalent stiffness of the single degree-of-freedom model. From the comparison, we see that IGA shows better accuracy than FEA under the same number of control points (or nodes used in FEA). Around 50% reduction of errors can be obtained from IGA. This is not only due to the geometric exactness of the NURBS representation but also the higher smoothness and polynomial order of it basis functions. In this case, since the quadratic NURBS functions are adopted, the NURBS basis functions are C^1 continuous compared with the C^0-continuous FEA shape functions.

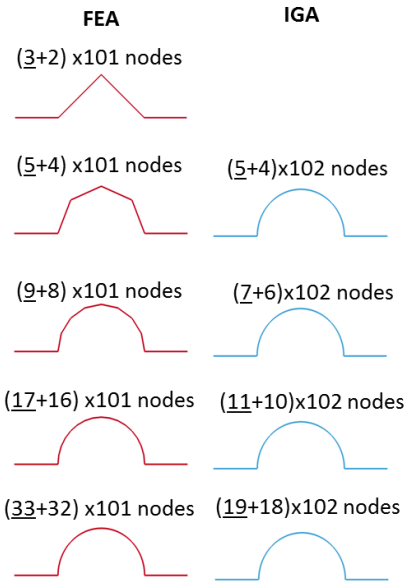

Figure 8. The cross-section profiles of FEA and IGA

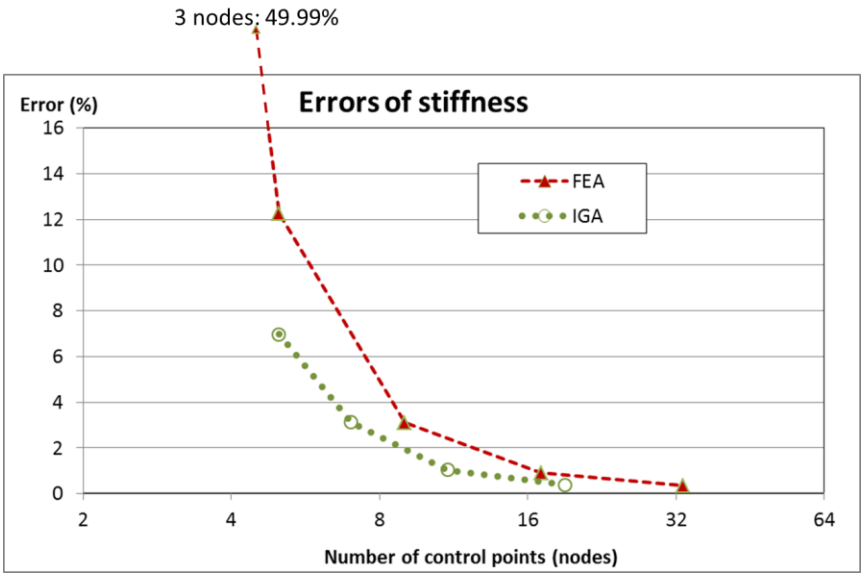

Figure 9. The comparison of errors of stiffness K_s between FEA and IGA

4.4. Multiple-patch NURBS model

There are issues connecting multiple patches in the NURBS-based IGA, in which the continuity of the NURBS basis functions on the boundaries of different patches will drop to C^0 or even less if weakly imposed connectivity is considered. The reduction of continuity will affect the accuracy in the CAE simulations. Here, the eigenvalue analysis of a simply supported square plate is considered as shown in Figure 10. The dimensions and the material properties of the square plate are also shown in the figure. Since the purpose is to consider the effects of multiple patches, Kirchhoff-Love assumption is adopted to avoid shear locking issue. Under the Kirchhoff-Love plate theory, the analytical solutions of the eigenvalues can be written as:

$$\omega_{mn} = \pi^2 \left(\frac{m^2}{a^2} + \frac{n^2}{b^2}\right) \sqrt{\frac{D}{\rho h}}, \qquad D = \frac{Eh^3}{12(1-v^2)} \tag{13}$$

where ω_{mn} is the natural frequency of this model.

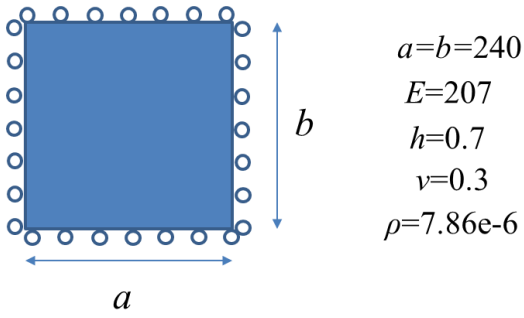

Figure 10. A simply supported square plate

In this example, 3 different numbers of patches are considered in NURBS-based IGA, they are 1, 4 and 16 patches in 2-D. Figure 11 shows the profiles of the quadratic NURBS basis functions with different numbers of patches. As can be seen, the continuity of the NURBS basis functions dropped from C^1 to C^0 for those intersected by the patch boundaries.

The frequency errors of IGA under different patches are compared with the ones from the FEA simulations as shown in Figure 12, where the error curves are re-interpolated based on the discrete modal frequency points by using linear polynomial-based reproducing kernel particle method (RKPM) **Error! Reference source not found.**]. In this example, the mesh size considered in the IGA model is 15 mm. However, for fair comparison, numbers of control points

in IGA and nodes in FEA are adopted as the basic criterion for performance comparison. Note that even if the same mesh size is used, IGA models with different numbers of patches have different numbers of control points. This is because the density of the control points near the patch boundaries will be higher than the ones away from the patch boundaries. Even if more control points are used for model with more patches, the accuracy is still reduced when patch numbers increased. This is due to the drop of the continuity as aforementioned. Still, the accuracy of IGA is still better than the one of FEA. As can be seen in Figure 12, IGA still performs better than FEA in this case. The FEA model with 1089 nodes show much larger error than all the IGA models no matter how many patches are used.

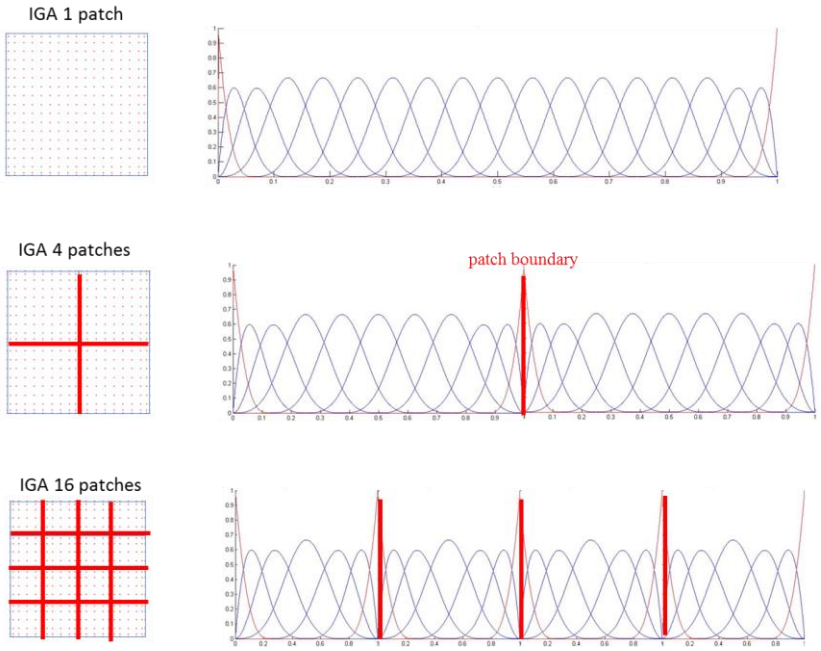

Figure 11. NURBS shape functions of models with different patch numbers

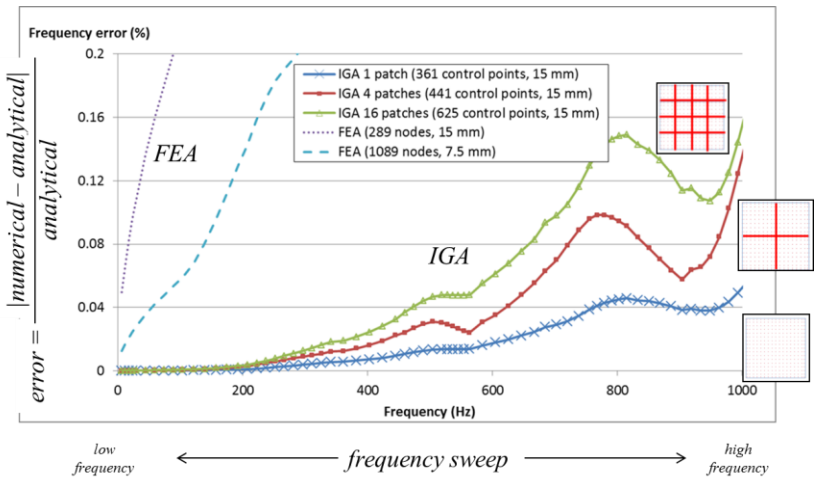

Figure 12. Comparison of IGA with different patch numbers and FEA

4.5. Other functionalities implemented in LS-DYNA IGA

To facilitate the construction of CAE model, there are some functionalities, which are related to IGA, implemented into the LS-PrePost and LS-DYNA as listed below:

(1) *Hybrid modeling of IGA and FEA*:

The fully implementation of IGA to replace current crash FEA is not practical in near future due to the existence of large database of barrier and dummy models. Thus, a hybrid of IGA-FEA modeling is tested and reported in this paper.

(2) *Imposition of initial constant velocity*:

The initial constant velocity of the IGA model can be directly imposed on the control points, since the NURBS basis functions possesses the partition of unity property, meaning any constant function can be exactly reproduced by the NURBS approximation.

(3) *Imposition of gravity or body force*:

The gravity or body force can be added through the keyword "*LOAD _BODY_(OPTION)". In the example of section 4.1, the uniformly distributed load q was the added as body force.

(4) *Connection by using spot weld*:

The spot welds in this paper are modeled as beam elements and connected to sheet metals (IGA patches) in meshless connecting manner by using the keyword

"*CONSTRAINED_NODE_TO_NURBS_PATCH_SET". More details will be shown in the example of crash safety simulations in the next section.

(5) *Connection by using extra nodes*:

"Extra node" of LS-DYNA rigid bodies is widely used to join parts to rigid body. The control points of IGA can be used as 'extra node' to connect to rigid body by using the keyword "*CONSTRAINED_EXTRA_ NODES_ SET". The implementation of extra nodes will be performed in the example of crash safety simulations in the next section.

(6) *Outputs of physical quantities*:

Since the NURBS basis functions do not possesses the Kronecker delta properties, the control points are not the physical points and can't be used to represent nodal physics such as accelerometers and DA (dimensional analysis) points. For these purposes, the keyword "CONSTRAINED_NODE_TO_NURBS_PATCH_SET" can be used to attach the additional nodes on the NURBS patches for outputs and then just as what is done in FEA, write out the histories of the attached nodes. This functionality will be used in the crash safety example. More details will be shown later.

(7) *Implementation of rigid wall*:

The implementation of contact of IGA parts with rigid wall is completed for IGA crash simulation. Just as the usage in FEA, the rigid wall can be added by using the keyword "RIGIDWALL_(OPTION)". This functionality will be also used in the crash safety example.

(8) *The contact of NURBS surfaces*:

Special contact algorithm including self-contact of NURBS surfaces is implemented through the keyword "*CONTACT_AUTOMATIC_SINGLE_SURFACE". It is used between the NURBS surfaces and to FEM elements.

5. Numerical Example of Crash Safety Simulation in LS-DYNA

A sled model as shown in Figure 13 was developed to demonstrate the features of IGA in crash safety simulation. Figure 14 illustrates the models in cross section and side views without and with holes. For the one with holes, trimmed NURBS surfaces are used to model this problem. Mindlin-Reissner plate theory is adopted in this example. A piecewise linear plastic material

model and the thickness of 1.7 mm are assigned to the front horn. The numerical results of the IGA-FEA hybrid models will be compared with the pure FEA models. Some functionalities of DYNA IGA have been used in this example. They are:

(1) Hybrid modeling of IGA and FEA is adopted in this example. The simplified front horn is modelled by using IGA, while the sled is modelled by using FEA.

(2) The initial velocity of -15.646 mm/ms is assigned to the sled and simplified front horn models.

(3) The spot welds are used to connect the two pieces of front horn components as shown in Figure 14.

(4) The front horn (deformable) and the sled (rigid) are connected by using the option of extra nodes from rigid body.

(5) The acceleration of a point is written out by attaching a node to the NURBS patch.

(6) The contact between the rigid wall and the NURBS surface is defined through the keyword "*RIGIDWALL_PLANAR" with zero friction.

(7) The contact of the front horn, spot welds and the sled is simply defined by using the keyword "*CONTACT_AUTOMATIC_SINGLE_SURFACE".

The details of the numerical results will be discussed in the next sub-sections.

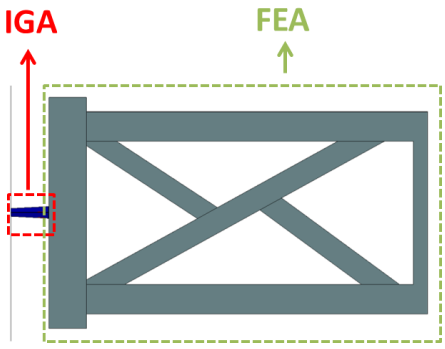

Figure 13. A CAE model to test basic crash simulation setups

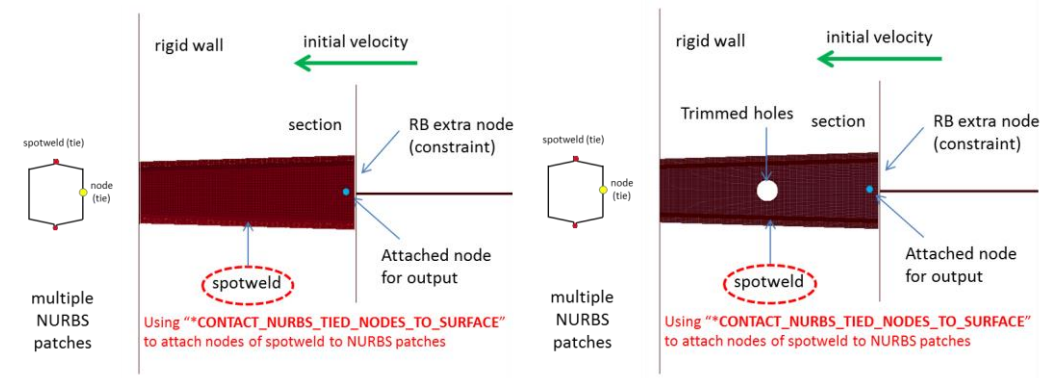

(a) without holes (b) with holes

Figure 14. The cross section and side views of the simplified front horn without holes

5.1. Untrimmed NURBS-based IGA Compared with FEA

To justify the accuracy of IGA, here we compare the numerical results between untrimmed NURBS-based quadratic IGA and linear FEA. Figure 15 shows the iso-metric view and top view of the deformation patterns of the test from IGA and FEA. Note that the numbers of degree of freedoms between FEA and IGA are about the same. The IGA mesh in Figure 15 is a finer mesh generated by LS-PrePost for post-processing purpose. In the current version of LS-PrePost, the mesh is obtained by subdividing the IGA mesh of the CAE model. As can be seen in Figures 13 and 14, this model is symmetric about the x-z plane, so we expect the deformed shape of the model should also be symmetric. However, the FEA seems to be more sensitive to modeling noise and the result does not show the symmetric modes of the crash test. Furthermore, the contact of IGA also works well as can be seen from the deformation plots. The self-contact of the NURBS surfaces and the contact among different components constructed based on different methods both function appropriately. The comparison of the deformation patterns between IGA and FEA demonstrates the superiority of NURBS-based IGA over FEA. NURBS-based IGA gives an symmetric deformation pattern due to its advantage in the geometric description and the high regularity of NURBA basis functions.

We further conduct the quantitative comparison between IGA and FEA. Figure 16 shows the rigid wall force histories of IGA and FEA. In Figure 16 (a), the rigid wall force of IGA is different from FEA, but the magnitudes of the rigid wall forces from the two different methods are around the same range.

To further justify that the IGA results are reasonable, we show the consistency between the IGA rigid wall force and the equivalent inertial force, which is obtained by using Newton's Second Law of motion, $F=ma$, where F is the equivalent inertial force, m is the mass of the sled and a is the acceleration of the attached node on the NURBS patch as shown in Figure 14. A SAE180 filter is used for the rigid wall force and acceleration histories to eliminate the noises.

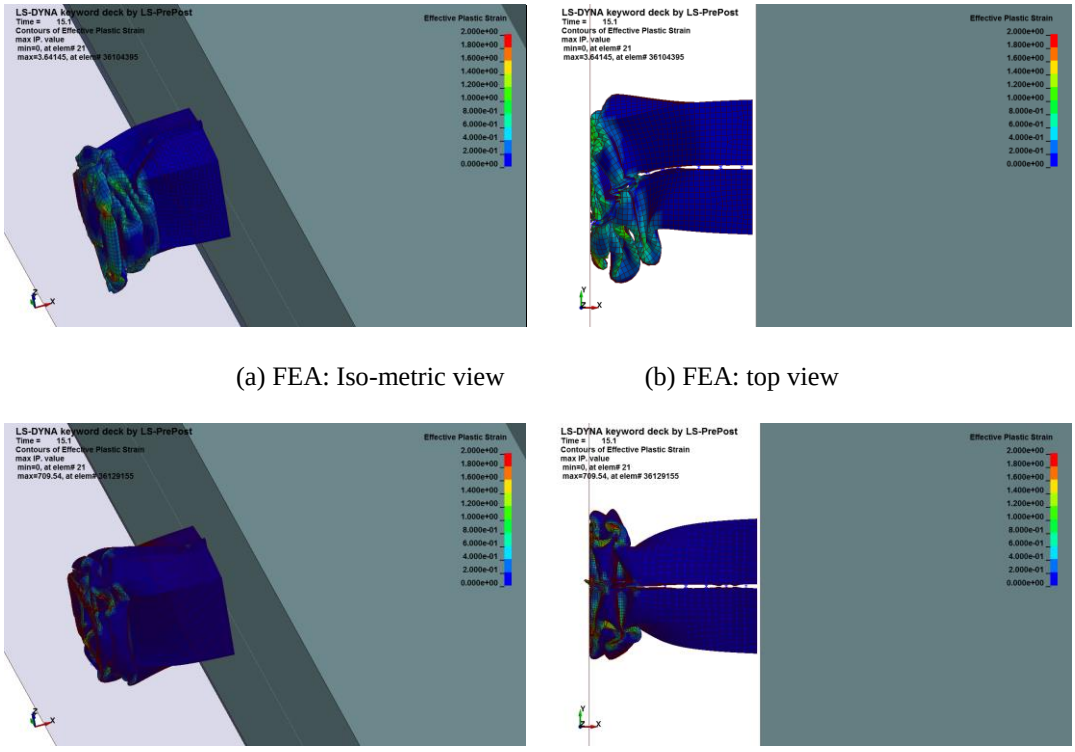

(a) FEA: Iso-metric view (b) FEA: top view

(c) IGA: Iso-metric view (d) IGA: top view

Figure 15. The deformation patterns of the front horn without holes from IGA and FEA

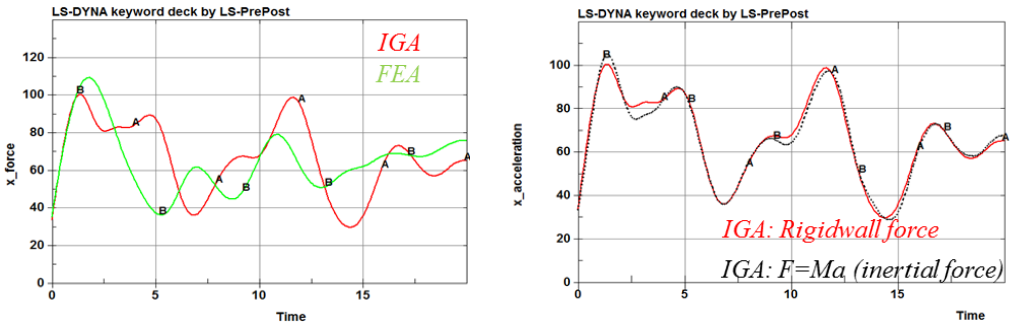

(a) Rigid wall forces of IGA and FEA (b) Consistency of IGA rigid wall force and inertial force

Figure 16. The time histories of rigid wall forces of IGA and FEA for the front horn without holes

5.2. Trimmed NURBS-based IGA Compared with FEA

The trimmed NURBS-based IGA has been also tested in this paper. The IGA front horn model with holes is built by using trimmed NURBS. The holes are defined by using trimming lines. As being aforementioned, using trimmed NURBS can significantly reduce the complexity of building CAE models. All the conditions for this case are the same as the previous case except for the trimmed holes. Figure 17 shows the final deformed configuration of FEA and IGA. Figure 18 shows the comparison of rigid wall forces between FEA and the trimmed NURBS-based IGA. Similar to the previous case, the magnitudes of the rigid wall forces from the two different methods are around the same range. Since the superiority of IGA has been justified in the previous case, there is no further comment in this example.

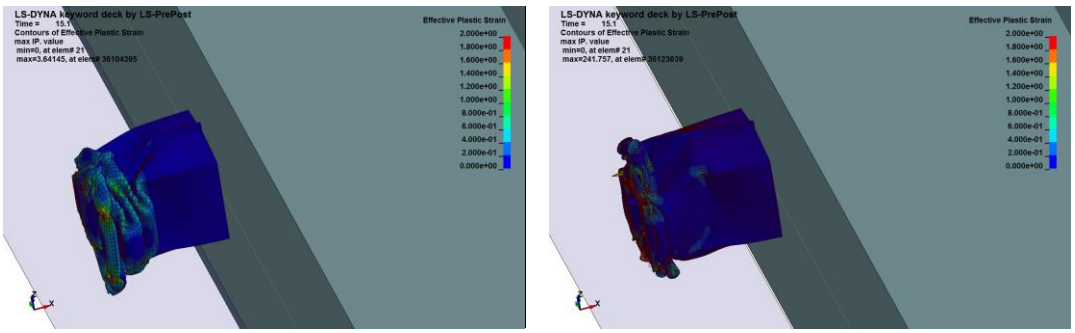

(a) FEA: Iso-metric view (b) IGA (trimmed NURBS): Iso-metric view

Figure 17. The deformation patterns of the front horn with holes from IGA and FEA

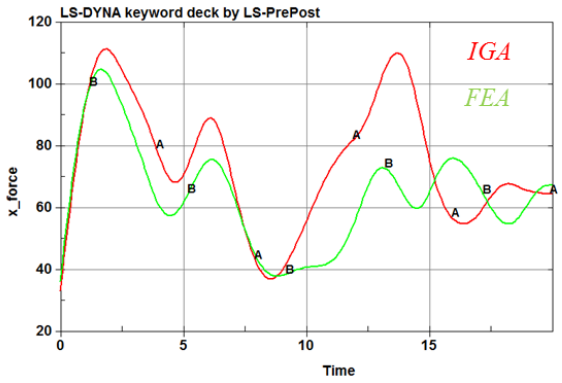

Figure 18. The time histories of rigidwall forces of IGA and FEA for the front horn with holes

6. Some Remaining Issues in LS-DYNA IGA

To illustrate the issues in the current DYNA-IGA, a crash model of a tapered cylinder is considered as shown in Figure 19. The moving rigid wall of 2000 kg is prescribed with velocity

16 m/s and the other end of the cylinder is clamped. The IGA model of the cylinder is constructed by using 3 patches. Note that in this case, although the geometry can be exactly represented by using NURBS-based approximation, the minimum number of patches used to describe the cylinder is 3 due to the nature of the NURBS basis. Hence, the model cannot be constructed by using only single patch. More details of the NURBS basis of this model are illustrated in Figure 20. Each of the 3 patches has a subtended angle 120° and on the patch boundaries the continuity drops to C^0. In this case, both the models based on Mindlin-Reissner and Kirchhoff-Love plate theories are considered to discuss the issues in the current DYNA-IGA.

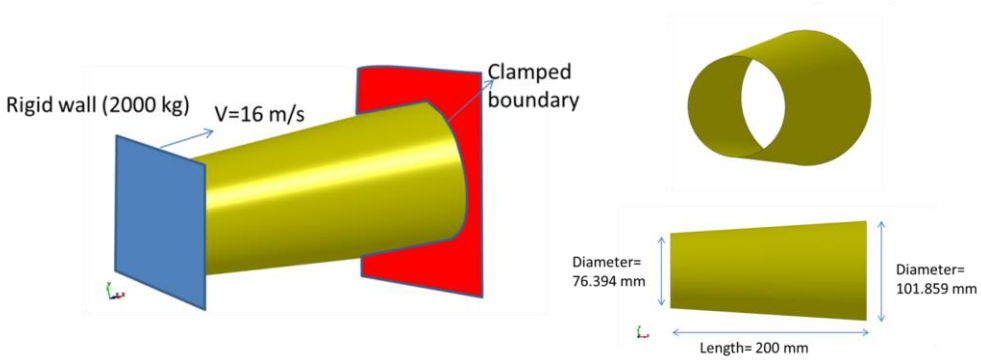

Figure 19. Crash test of a tapered cylinder

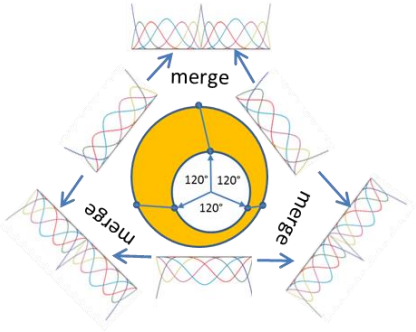

Figure 20. The NURBS basis of the tapered cylinder

6.1. Model Based on the Mindlin-Reissner Plate Theory

In the first case, we compare the models of IGA and FEA based on the Mindlin-Reissner plate theory. For the implementation in LS-DYNA, FEA with form 16 and IGA with form 0 are chosen for modeling this problem. To relive the shear locking effect, cubic NURBS basis functions are

selected for the approximations of the displacement and rotation fields. Figure 21 shows the deformed configurations of the numerical results from IGA and FEA with mesh size 2.0 mm.

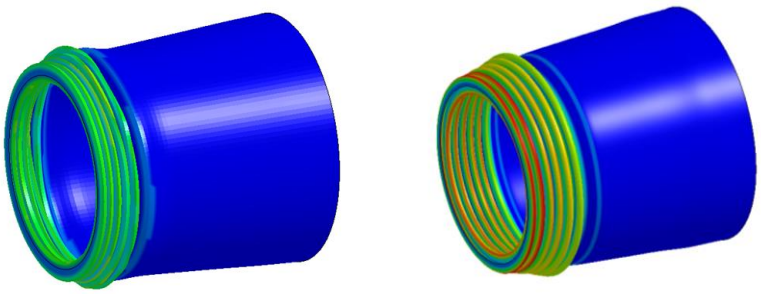

(a) FEA form 16 with mesh size 2.0 mm (b) IGA form 0 with mesh size 2.0 mm

Figure 21. The deformed configurations of the tapered cylinder from IGA form 0 and FEA

As can be seen from Figure 21, the folding of the IGA model is smoother than that of FEA due to the high smoothness provided by the cubic NURBS basis functions. IGA result also shows a perfect axial symmetry of the folding compared to FEA result due to its exact description of the conic geometry. As we further compare the rigid wall forces of FEA and IGA as shown in Figures 22 and 23, we can see that both FEA and IGA converge. However, the FEA and IGA models give different solutions of the rigid wall forces for this example, although converged solutions are obtained from both methods. This might be an issue to justify the accuracy of IGA. To justify the accuracy of IGA, the solutions might need to be compared with the results from experiments, but so far there is no experiment available for the validation of IGA.

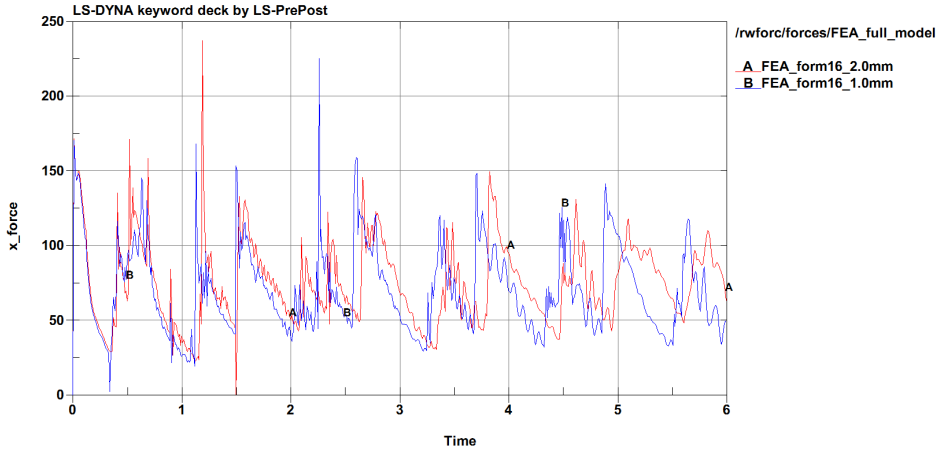

Figure 22. The rigidwall forces of FEA models with different discretizations

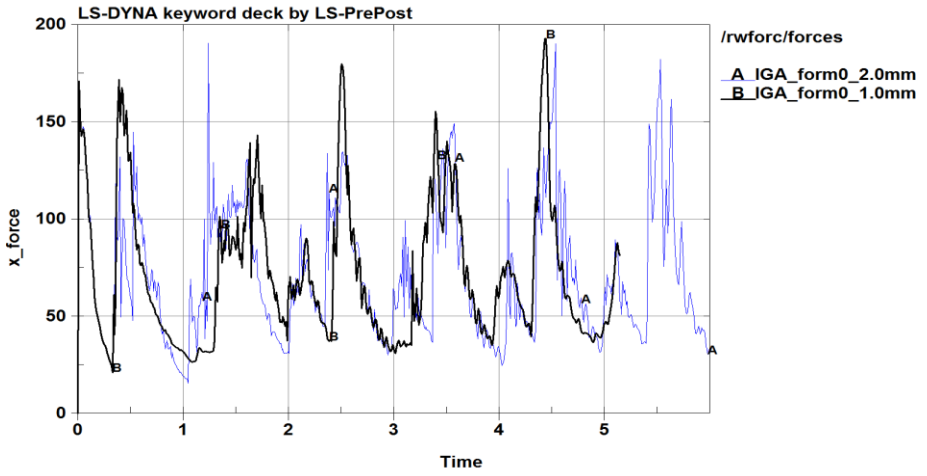

Figure 23. The rigid wall forces of IGA form 0 models with different discretization

For current DYNA IGA, its run time is not compatibility to FEA as shown in Figure 24. The quick drop of time step in the early stage IGA run starting from the first folding of the crash can may be the root cause of small time step and the resulting of long run time. The parallel computing of IGA in the current LS-DYNA is not optimized yet. It may also contribute to the long run time of IGA.

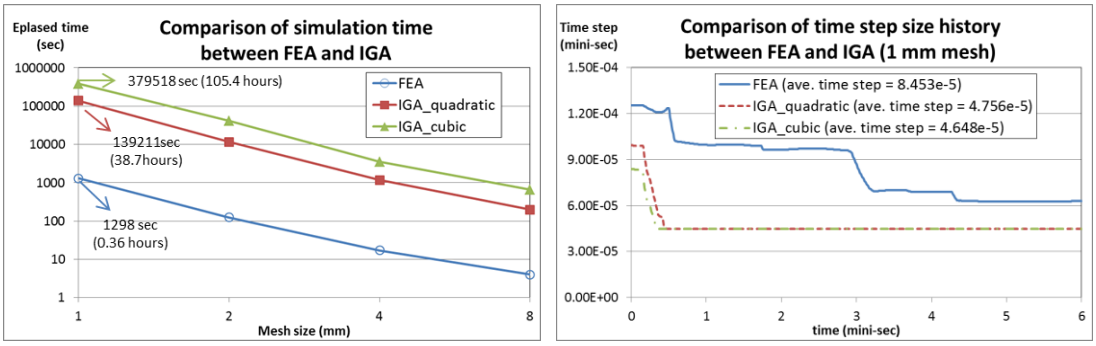

(a) Simulation time of FEA and IGA (b) Histories of the time step size of FEA and IGA

Figure 24. Computational efficiency of FEA and IGA

There is a secondary issue about the functionality in the current LS-DYNA. The section force calculation in the current DYNA-IGA is not available yet. Figure 25 shows the section force of the IGA model, where the section force history is zero due to its unavailability in the current version of LS-DYNA.

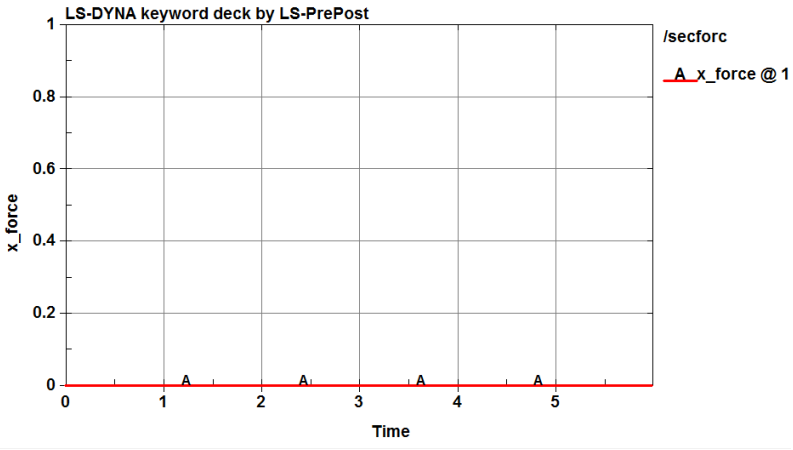

Figure 25. The section force history of IGA

6.2. Model Based on the Kirchhoff-Love Plate Theory

There is another choice for analyzing this problem, which is to build the CAE model based on the Kirchhoff-Love plate theory. In this case, quadratic and cubic IGA with form -4 are chosen for modeling this problem. However, Kirchhoff-Love plate theory requires the approximation basis to be at least C^1 continuous for the entire domain, while the minimum patch number for the cylinder is three, meaning the continuity across the patch boundaries is C^0. IGA form -4 is not purely based on the Kirchhoff-Love plate theory. Instead, it's a hybrid approach. For the region near the patch boundaries, Mindlin-Reissner plate theory is applied which only requires C^0 continuity, while for the region away from the patch boundaries Kirchhoff-Love plate theory is adopted for the CAE modeling. Since as fine discretization is used, the region near the patch boundary will be very small, therefore the general behaviors of this problem will be more similar to the Kirchhoff plate.

Figure 26 shows the deformed configurations and the corresponding plastic strain contours of the quadratic and cubic IGA form -4 models. From Figure 26 (b), the instability is observed. The numerical result becomes unreliable since the instability occurs. Hence, to adopt the Kirchhoff plate model, the instability issue in the DYNA-IGA needs to be resolved. Currently, the cause of the instability is not identified.

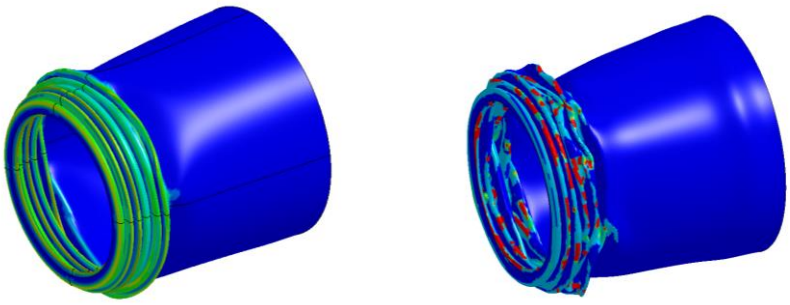

(a) Quadratic IGA (b) Cubic IGA

Figure 26. The deformed configurations of the tapered cylinder from IGA form -4

6.3. Summary of the Remaining Issues

According to the numerical results of this example, we summarize the issues observed in the current DYNA IGA as listed below:

(1) Section force calculation is unavailable.

(2) Converged IGA solution is different from the converged FEA solution.

(3) The efficiency of IGA needs to be further enhanced.

(4) The instability issue in IGA form-4 needs to be resolved.

7. Conclusions

In this paper, the current status of the DYNA IGA has been reported. In general, crash simulations of models with simple geometry can be analyzed by using DYNA IGA. Basic functionalities have been implemented to the current version of LS-DYNA for crash simulations. IGA, in terms of accuracy, shows the superior performance over the conventional FEA as being demonstrated in the numerical examples. The computational cost of IGA is still higher than. Furthermore, more numerical studies are required to justify the accuracy of IGA, since IGA offers different solutions from FEA in the given examples. A DYNA-IGA based Bézier extraction is available to interface with advanced spline methods. It is believed to have similar advantages as current NURBS based IGA. Further investigation is required to explore its benefit in auto design process. Some other issues related to the functionalities of DYNA IGA also need to be resolved as being mentioned in this paper. Additionally, IGA can provide more facility during the design stage due to the direct CAD-CAE communication, which can hugely reduce the time cost during the design cycles.

8. Acknowledgment

This study is supported by Ford PMIT 2015 funding. This paper covers the IGA studies in crash safety. The authors acknowledge Randy Frank, CAE Chief Engineer and James Cheng, Passive

Safety Manager in R&A for their support and encouragement. Special thanks are due to Dilip Bhalsod of LSTC for his continuous help in resolving many issues the team faced during the IGA analysis of the problems included in this paper. Also we thank Dr. David Benson, Dr. Stefan Hartmann, Dr. Philip Ho and Dr. Isheng Yeh for the critical technical support the team received during the course of this study.

References

[1] Hughes, T. J., Cottrell, J. A., & Bazilevs, Y. (2005). Isogeometric analysis: CAD, finite elements, NURBS, exact geometry and mesh refinement. Computer methods in applied mechanics and engineering, 194(39), 4135-4195.

[2] Cottrell, J. A., Hughes, T. J., & Bazilevs, Y. (2009). Isogeometric analysis: toward integration of CAD and FEA. John Wiley & Sons.

[3] Bazilevs, Y., Calo, V. M., Hughes, T. J. R., & Zhang, Y. (2008). Isogeometric fluid-structure interaction: theory, algorithms, and computations. Computational mechanics, 43(1), 3-37.

[4] Bazilevs, Y., Calo, V. M., Cottrell, J. A., Evans, J. A., Hughes, T. J. R., Lipton, S., Scott, M. A. a& Sederberg, T. W. (2010). Isogeometric analysis using T-splines. Computer Methods in Applied Mechanics and Engineering, 199(5), 229-263.

[5] Giannelli, C., Jüttler, B., Kleiss, S. K., Mantzaflaris, A., Simeon, B., & Špeh, J. (2015). THB-splines: An effective mathematical technology for adaptive refinement in geometric design and isogeometric analysis. Computer Methods in Applied Mechanics and Engineering.

[6] Benson, D. J., Bazilevs, Y., Hsu, M. C., & Hughes, T. J. R. (2010). Isogeometric shell analysis: the Reissner–Mindlin shell. Computer Methods in Applied Mechanics and Engineering, 199(5), 276-289.

[7] Benson, D. J., Bazilevs, Y., Hsu, M. C., & Hughes, T. J. R. (2011). A large deformation, rotation-free, isogeometric shell. Computer Methods in Applied Mechanics and Engineering, 200(13), 1367-1378.

[8] Piegl, L. and W. Tiller, The NURBS book. 1995, New York: Springer.

[9] Hughes, T. J., Cohen, M., & Haroun, M. (1978). Reduced and selective integration techniques in the finite element analysis of plates. Nuclear Engineering and Design, 46(1), 203-222.

[10] Belytschko, T., Stolarski, H., Liu, W. K., Carpenter, N., & Ong, J. S. (1985). Stress projection for membrane and shear locking in shell finite elements. Computer Methods in Applied Mechanics and Engineering, 51(1), 221-258.

[11] Caseiro, J. F., Valente, R. A. F., Reali, A., Kiendl, J., Auricchio, F., & De Sousa, R. A. (2014). On the Assumed Natural Strain method to alleviate locking in solid-shell NURBS-based finite elements. Computational Mechanics, 53(6), 1341-1353.

[12] Bouclier, R., Elguedj, T., & Combescure, A. (2012). Locking free isogeometric formulations of curved thick beams. Computer Methods in Applied Mechanics and Engineering, 245, 144-162.

[13] Liu, W. K., Jun, S., & Zhang, Y. F. (1995). Reproducing kernel particle methods. International journal for numerical methods in fluids, 20(8-9), 1081-1106.

[14] Sederberg, T. W., Cardon, D. L., Finnigan, G. T., North, N. S., Zheng, J., & Lyche, T. (2004). T-spline simplification and local refinement. In Acm transactions on graphics (tog) (Vol. 23, No. 3, pp. 276-283). ACM. International journal for numerical methods in fluids, 20(8-9), 1081-1106.

[15] Borden, M. J., Scott, M. A., Evans, J. A., & Hughes, T. J. (2011). Isogeometric finite element data structures based on Bézier extraction of NURBS. International Journal for Numerical Methods in Engineering, 87(1-5), 15-47.

[16] Scott, M. A., Borden, M. J., Verhoosel, C. V., Sederberg, T. W., & Hughes, T. J. (2011). Isogeometric finite element data structures based on Bézier extraction of T-splines. International Journal for Numerical Methods in Engineering, 88(2), 126-156. (10 point Times New Roman)